FROM MICRO-CT TO MULTISCALE MECHANICS OF DOUBLE-POROUS HYDROXYAPATITE GRANULES FOR REGENERATIVE MEDICINE

Alexander Dejaco
Institute for Mechanics of Materials and Structures
Vienna University of Technology
Karlsplatz 13/202, A-1040 Vienna, Austria

Vladimir S. Komlev
InMatrixs Ltd
Lyalin per., 21, bld. 2, 103062 Moscow, Russia

Jakub Jaroszewicz
Department of Materials Science and Engineering
Warsaw University of Technology
Wołska 141, 02-507 Warsaw, Poland

Wojciech Swieszkowski
Department of Materials Science and Engineerin
Warsaw University of Technology
Wołska 141, 02-507 Warsaw, Poland

Christian Hellmich
Institute for Mechanics of Materials and Structures
Vienna University of Technology
Karlsplatz 13/202, A-1040 Vienna, Austria

Alex N. Gurin
Central Scientific Research Institute of Dentistry
and Maxillo-facial Surgery
Timura Frunze 16, 119991, Moscow, Russia

ABSTRACT

Hundred micrometers-sized porous hydroxyapatite globules have proved as successful tissue engineering strategy for bone defects *in vivo*, as was shown in studies on human mandibles. These granules need to provide enough porous space for bone ingrowth, while maintaining sufficient mechanical competence (stiffness and strength) in this highly load-bearing organ. This double challenge motivates us to scrutinize more deeply the micro and nanomechanical characteristics of such globules, as to identify possible optimization routes. Therefore, we imaged such a (pre-cracked) granule in a microCT scanner, transformed the attenuation coefficients into voxel-specific nanoporosities, from which we determined, via polycrystal micromechanics, voxel-specific (heterogeneous) elastic properties. The importance of the latter and of the presence of one to several hundred micrometers-sized cracks for realistically estimating the load-carrying behavior of the globule under a typical two-point compressive loading (as in a "splitting" test) is shown through results of large-scale Finite Element analyses, in comparison to analytical results for a sphere loaded at its poles: Use of homogeneous instead of heterogeneous elastic properties would overestimate the structure's stiffness by 5% (when employing a micromechanics-based process as to attain homogeneous properties) - the cracks, in comparison, weaken the structure by one to two orders of magnitudes.

KEY WORDS

Hydroxyapatite, Finite Element Analysis, Polycrystal Micromechanics, Computed Tomography.

1 Introduction

Hydroxyapatite (HA) is broadly used as a base component for synthetically built biomaterials and tissue engineering scaffolds.

Given their role in the load-carrying function of the vertebrate skeleton, the mechanical properties of hydroxyapatite materials and structures are of imminent interest.

Extending and adapting our earlier strategy developed for glass-based biomaterials [1], we here simulate the elastic behavior of hydroxyapatite granules used for regeneration of bone defects in a clinical framework [2]. We start with a micro Computer Tomographic image of the object, and first translate, based on the average rule for X-ray attenuation coefficients [3, 4], the voxel-specific attenuation values into voxel-specific nanoporosities. Subsequently, we propose a multiscale elastic analysis: we use semianalytical random homgenization methods [5] to predict the elasticity of RVEs of several microns characteristic length, from the elastic properties of single (elongated) hydroxyapatite crystals and the nanoporosity inbetween [6, 7, 8]. Subsequently, these RVEs are represented by Finite Elements in a structural analysis of one hydroxyapatite granule, subjected to compressive forces at its poles, as experienced in a "splitting test" [9]. In this way, we aim at answering the following questions: (1) how large are the effects of the scaffold-microinhomogeneity when estimating the stresses at the level "felt" by biological cells?, and (2) how do these effects compare to effects related to cracks with lengths similar to or larger than those of biological cells?

2 Materials and Methods

The granules of carbonate-containing hydroxyapatite (CHA) were prepared according to the processing route de-

scribed in [2]. This technology allows for the production of spherical CHA granules with widely ranging diameters, from 50 to about 2000 microns. These globules contain pores of two sizes: the larger ones are in the order of one to several hundred micrometers ("micropores"), while the smaller ones have a characteristic size of less than one micron ("nanopores").

In the used micro-CT reconstruction algorithm, realized in SKYSCAN's NRecon v1.6.1.2 software, a beam hardening correction of 50% and a ring artefact correction of 20 were chosen, leading to satisfactory image quality (see Fig. 1). In the reconstructed image slices, the voxel-specific X-ray attenuation coefficients μ are given in terms of grey values X, according to the linear relation
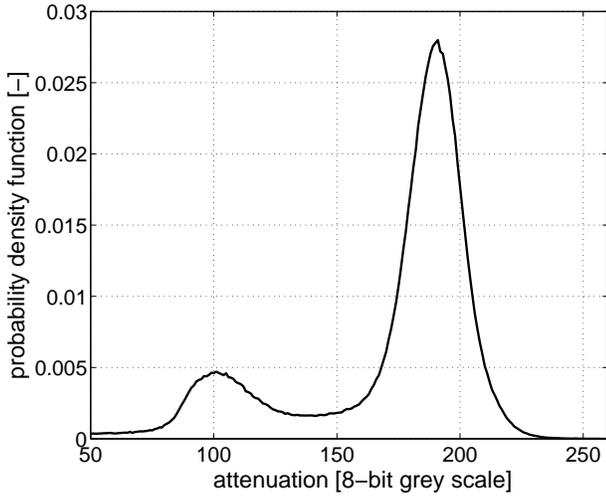

Figure 2: Statistical characteristics of μCT image of porous hydroxyapatite granule depicted in Fig. 1: probability density function of attenuation (in terms of grey values)

$$X = a \times \mu + b \tag{1}$$

with a and b being proportionality constants. Next, we translate such voxel-specific grey values to voxel-specific nanoporosities ϕ_{nano}. Therefore, we consider the average rule for attenuation coefficients of composite materials [3, 1, 4], reading for our case as

$$\mu = \phi_{nano}\mu_{air} + (1 - \phi_{nano})\mu_{HA} \tag{2}$$

with μ_{air} as the X-ray attenuation coefficient of air filling the nanoporous space, and with μ_{HA} as the X-ray attenuation coefficient of pure hydroxyapatite. Inserting (1) into (2) yields an average rule for grey values, reading as

$$X = \phi_{nano}X_{air} + (1 - \phi_{nano})X_{HA} \tag{3}$$

which can be transformed, as to provide the voxel-specific nanoporosity from grey values, in the form

$$\phi_{nano}(X) = \frac{X - X_{HA}}{X_{air} - X_{HA}} \tag{4}$$

with X_{air} as the grey value of an air-filled voxel, and X_{HA} as the grey value of a voxel which is totally filled by pure (dense) hydroxyapatite. $X_{air} = 100$ can be identified from the "air peak" of a grey value histogram (see Fig. 2), and we use the minimum value between the "air peak" and the "solid peak" in Fig. 2 as the threshold $X_{thr} = 139$ to delineate between pure "air voxels" (with $X < X_{thr}$) and "solid voxels" ($X > X_{thr}$), the latter containing a nanoporosity according to (4). Hence, we have

$$\phi_{nano}(X) = \frac{X - X_{HA}}{X_{air} - X_{HA}} \text{ for } X > X_{thr} \tag{5}$$

and

$$\phi_{nano}(X) = 1 \text{ for } X < X_{thr} \tag{6}$$

The (normalized) histogram of Fig. 2 does not contain any voxel which is totally filled with pure hydroxyapatite, since the single hydroxyapatite crystals are much smaller than the voxel size of 3.49 microns. Hence, we are left with finding a way to identify X_{HA}, which, according to the aforementioned considerations, is larger than 255. Therefore, we consider, as additional quantity, the total porosity of the investigated globule, i.e. the entire space occupied by both nanopores and micropores, over the space occupied by the entire (double-porous) globule. The total porosity is known from the mass and the volume of the globule, as well as from the mass density of pure hydroxyapatite: in the present case, it amounts to $\Phi_{total} = 0.55$. The total porosity (air space in globule over total volume of globule) is related to the voxel-specific nanoporosity ϕ_{nano} via

$$\Phi_{total} = \int_0^{255} p(X)\phi_{nano}(X)\,dX \tag{7}$$

with $p(X)$ as the probability density function of grey-scaled attenuation values X depicted in Fig. 2. Use of (5) and (6) in (7) yields

$$\Phi_{total} = \int_{X_{thr}}^{255} p(X)\frac{X - X_{HA}}{X_{air} - X_{HA}}\,dX + \int_0^{X_{thr}} p(X)\,dX =$$
$$= \int_{X_{thr}}^{255} p(X)\phi_{nano}(X)\,dX + \Phi_{micro} \tag{8}$$

within the globule, $\Phi_{micro} = 0.189$. Transformation of (8) gives access to the sought grey value of pure (dense) hydroxyapatite, X_{HA}, as

$$X_{HA} = \frac{1}{1 - \Phi_{total}} \times \tag{9}$$
$$\times \left\{ X_{air}(\Phi_{micro} - \Phi_{total}) + \int_{X_{thr}}^{255} p(X)X\,dX \right\}$$

$X_{HA} = 257.9$ in our case, i.e. the smallest nanoporosity amounts to $\phi_{nano}^{min} = 0.018$ [according to (4)].

Different amounts of neighboring voxels (namely $4 \times 4 \times 4 = 64$ voxels, $5 \times 5 \times 5 = 125$ voxels, $7 \times 7 \times 7 = 343$ voxels, $8 \times 8 \times 8 = 512$ voxels, $9 \times 9 \times 9 = 729$ voxels, $10 \times 10 \times 10 = 1000$ voxels, $12 \times 12 \times 12 = 1728$
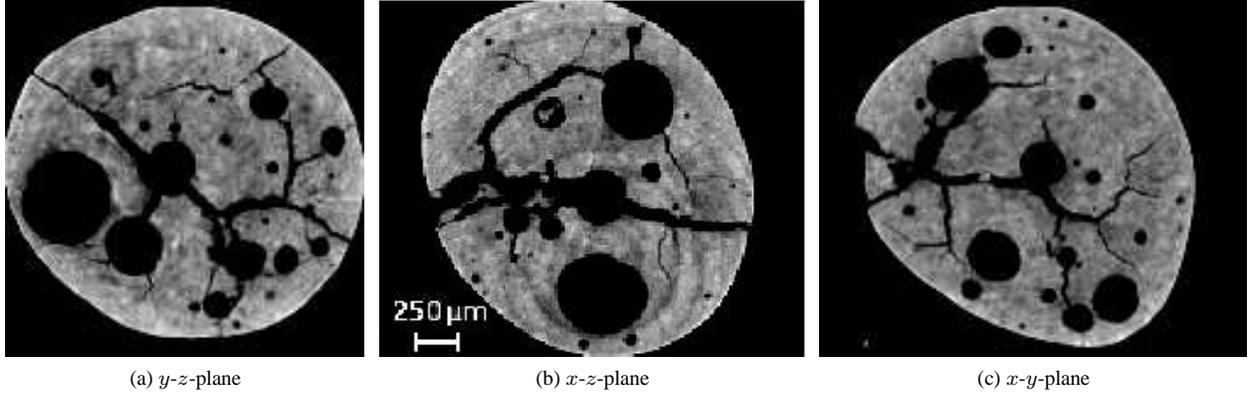
(a) y-z-plane   (b) x-z-plane   (c) x-y-plane

Figure 1: μCT-images of investigated granule: three perpendicular cross sections through the center of the granule, labelled through a right-handed x,y,z-coordinate system: (a) y-z plane, (b) x-z plane, (c) x-y plane

voxels, $15 \times 15 \times 15 = 3375$ voxels, $20 \times 20 \times 20 = 8000$ voxels, and $30 \times 30 \times 30 = 27000$ voxels) were merged into cubic Finite Elements (FE), which were assigned the mean grey-scaled attenuation value averaged over all the merged voxels. If this mean attenuation value was below X_{thr}, the respective Finite Element was skipped, otherwise it was assigned a nanoporosity according to Eq. (4).

Next, each Finite Element-specific nanoporosity is translated into Finite Element-specific isotropic elastic properties, by means of the micromechanical model of Fritsch et al. [7] for porous polycrystals built up by elongated hydroxyapatite crystal phases oriented in all space directions, developed in the framework of so-called random homogenization theory or continuum micromechanics [5].

Given the load-bearing function of such globules in a pile with globule-to-globule contact (situated in a bone defect), we consider, as the very first load case applied to this material system in a virtual environment, "uniaxial" compression in form of slightly distributed forces on both "poles" of the globule, which is realized in terms of prescribed displacements in the loading direction, amounting to zero at one side of the globule, and amounting to 0.1% of the globule diameter, at the other. The magnitude of the prescribed displacement is chosen as to mimic normal physiological strain states characterized by the order of 1000 microstrains [10, 11, 12]. The results of the Finite Element simulations in Abaqus Version 6.7-2, are reported in terms of the forces acting at the poles (reaction forces), of element-specific strains and stresses throughout the structure, as well as of stress/strain averages (first and second-order moments) over the (solid) elements. More specifically, we evaluate the Finite Element-specific norm of the deviatoric stress

$$\sigma_{dev}(\boldsymbol{x}) = \sqrt{\frac{1}{2}\boldsymbol{\sigma}_{dev}(\boldsymbol{x}) : \boldsymbol{\sigma}_{dev}(\boldsymbol{x})} \qquad (10)$$

whereby the deviatoric stress tensor is standardly defines as

$$\boldsymbol{\sigma}_{dev}(\boldsymbol{x}) = \boldsymbol{\sigma}(\boldsymbol{x}) - \mathbf{1}\,tr[\boldsymbol{\sigma}(\boldsymbol{x})] \qquad (11)$$

where $\boldsymbol{\sigma}$ is the Cauchy stress tensor, $\boldsymbol{x}$ gives the position of the considered Finite Element, tr is the trace operator, and $\mathbf{1}$ is the second-order unity tensor. Additionally, the first-order average of stresses over the domain of solid Finite Elements is evaluated according to [13]

$$\bar{\sigma}_{dev} = \sqrt{\frac{1}{2}\langle\boldsymbol{\sigma}_{dev}(\boldsymbol{x})\rangle : \langle\boldsymbol{\sigma}_{dev}(\boldsymbol{x})\rangle} \qquad (12)$$

with

$$\langle(.)\rangle = \frac{1}{V_s}\int_{V_s}(.)\,\mathrm{d}V \qquad (13)$$

as the average of quantity $(.)$ over all (solid) Finite Elements, filling volume V_s. The second-order average of stresses is evaluated as [13]

$$\bar{\bar{\sigma}}_{dev} = \sqrt{\frac{1}{2}\langle\boldsymbol{\sigma}_{dev}(\boldsymbol{x}) : \boldsymbol{\sigma}_{dev}(\boldsymbol{x})\rangle} \qquad (14)$$

As to answer the mechanical questions concerning nanoporosity distributions and cracks, as stated in the Introduction, two types of comparisons are made:

- For assessing the influence of nanoporosity distribution over the globule, results of the aforementioned Finite Element model with voxel-specific elastic properties are compared to results from a Finite Element model where all solid elements exhibit the mean nanoporosity averaged over all solid voxels (with $X > X_{thr}$), amounting to $\bar{\phi}_{nano} = 0.445$; the corresponding Young's modulus amounts to $E_{PHA}(\bar{\phi}_{nano}) = 23.8$ GPa.

- For assessing the influence of one to several hundred micrometers-sized cracks, the results of the aforementioned simulations are compared to the analytical solution for spheres compressed at their poles, whereby the material building up the spheres consists of a matrix with elastic properties corresponding to the mean

	heterogeneous	homogeneous
	value [Pa]	value [Pa]
$\bar{\sigma}_{dev}$	$8.68 \cdot 10^5$	$9.14 \cdot 10^5$
$\bar{\bar{\sigma}}_{dev}$	$4.89 \cdot 10^6$	$4.66 \cdot 10^6$

Table 1: First and second order moments of deviatoric stresses, for homogeneous and heterogeneous (element-specific) elastic properties

	heterogeneous	homogeneous
component	value [N]	value [N]
R_{xx}	0.343	0.277
R_{yy}	0.189	0.167
R_{zz}	1.386	1.454

Table 2: Reaction forces at the poles of the granule, for homogeneous and heterogeneous (element-specific) elastic properties

nanoporosity of $\bar{\phi}_{nano} = 0.445$, with spherical micropores (but no cracks) being embedded into the aforementioned matrix (these micropores filling a microporosity of $\Phi_{micro} = 0.189$). The elastic properties of such a material are determined by the well-known Mori Tanaka method [14, 15], and its shear modulus, amounting to $G = 6.45$ GPa, enters the analytical formula of Lurje for a homogeneous sphere subjected to forces at its poles [16]

$$Z = \frac{\Delta r \cdot G \cdot r_0}{-0.127} \quad (15)$$

where Z gives the (compressive) force at the poles of the sphere (reaction force). This force is compared to the results of the FE simulations. Δr depicts the change in radius that was applied as displacement, and r_0 the original granule radius.

3 Results and Discussion

The forces needed to compress the heterogeneous granule are by 5% smaller than those needed to compress a globule with homogeneous solid properties derived from the mean nanoporosity in all solid Finite Elements (see Tab. 2). Hence, neglection of the heterogeneity in the solid leads to some overestimation of the global stiffness of the investigated granule. This difference in global stiffness is consistent with the first-order moment of deviatoric stresses in the (solid) Finite Elements, being larger in the homogeneous than in the heterogeneous simulations. On the other hand, the variability of different stress states throughout the solid Finite Elements is larger in the heterogeneous analysis, when compared to the homogeneous analysis, which can be seen from the second-order moments of deviatoric stresses (see Tab. 2), as well as from the histogram of

the deviatoric stress norms (see Fig. 4) and of the maximum principal stress (largest eigenvalue of stress tensor, see Fig. 3). Distribution plots of deviatoric stress norms and maximum principal stresses throughout the considered structure (see Fig. 5 and 6), reveal that stress peaks occur at the load introduction areas, and around crack-like structures, rather than close to the walls of pseudo-spherically shaped micropores. Given the remarkable, but rather small influence of nanoporosity distribution on the overall stiffness, the absence of crack-like features would leave only the micropores as effective reducers of global stiffness. A corresponding reaction force of $Z = 112$ N [estimated from Eq. (15)], being approximately 80 times larger than those from heterogeneous and homogeneous Finite Element analyses, clearly identifies the crack-like features in the investigated globule as the by far dominant stiffness-governing feature.

This reminds us of the pivotal role that cracking may play in activating high strains at the tens-of-micrometers level, which may trigger biological cells to initiate biochemical cascades inducing new bone formation [17]. In this context, (controlled) cracking of hydroxyapatite granules might even ease their successful integration into the natural skeletal system. However, the modeling of cracking processes as such is clearly beyond the present study, which is limited to linear elasticity. As a worthwhile next step, micro-elasto-brittle models [18, 8] could be used to study, at the structural level of one globule, typical cracking events induced by excessive loading. This is planned for the future.

4 Acknowledgment

References

[1] S. Scheiner, R. Sinibaldi, B. Pichler, V. Komlev, C. Renghini, C. Vitale-Brovarone, F. Rustichelli, and C. Hellmich, "Micromechanics of bone tissue-engineering scaffolds, based on resolution error-cleared computer tomography," *Biomaterials*, vol. 30, no. 12, pp. 2411–2419, 2009.

[2] V. S. Komlev, S. M. Barinov, and E. V. Koplik, "A method to fabricate porous spherical hydroxyapatite granules intended for time-controlled drug release," *Biomaterials*, vol. 23, no. 16, pp. 3449–3454, 2002.

[3] E. Crawley, W. Evans, and G. Owen, "A theoretical analysis of the accuracy of single-energy CT bone measurements," *Physics in Medicine and Biology*, vol. 33, no. 10, pp. 1113–1127, 1988.

[4] C. Hellmich, C. Kober, and B. Erdmann, "Micromechanics-based conversion of ct data into anisotropic elasticity tensors, applied to fe simulations of a mandible," *Annals of Biomedical Engineering*, vol. 36, pp. 108–122, 2008.

[5] A. Zaoui, "Continuum micromechanics: Survey," *Journal of Engineering Mechanics*, vol. 128, no. 8, pp. 808–816, 2002.

[6] A. Fritsch, L. Dormieux, C. Hellmich, and J. Sanahuja, "Mechanical behavior of hydroxyapatite biomaterials: An experimentally validated micromechanical model for elasticity and strength," *Journal of Biomedical Materials Research Part A*, vol. 88A, no. 1, pp. 149–161, 2009.

[7] A. Fritsch, L. Dormieux, and C. Hellmich, "Porous polycrystals built up by uniformly and axisymmetrically oriented needles: homogenization of elastic properties," *Comptes Rendus Mécanique*, vol. 334, no. 3, pp. 151–157, 2006.

[8] A. Fritsch, C. Hellmich, and L. Dormieux, "The role of disc-type crystal shape for micromechanical predictions of elasticity and strength of hydroxyapatite biomaterials," *Philosophical Transactions of the Royal Society A: Mathematical, Physical and Engineering Sciences*, vol. 368, no. 1917, pp. 1913–1935, 2010.

[9] C. Rocco, G. V. Guinea, J. Planas, and M. Elices, "Review of the splitting-test standards from a fracture mechanics point of view," *Cement and Concrete Research*, vol. 31, no. 1, pp. 73–82, 2001.

[10] M. Viceconti and A. Seireg, "A generalized procedure for predicting bone mass regulation by mechanical strain," *Calcified Tissue International*, vol. 47, no. 5, pp. 296–301, 1990.

[11] D. Taylor, "Fatigue of bone and bones: An analysis based on stressed volume," *Journal of Orthopaedic Research*, vol. 16, pp. 163–169, 1998.

[12] Y.-F. Hsieh, A. G. Robling, W. T. Ambrosius, D. B. Burr, and C. H. Turner, "Mechanical loading of diaphyseal bone in vivo: The strain threshold for an osteogenic response varies with location," *Journal of Bone and Mineral Research*, vol. 16, no. 12, pp. 2291–2297, 2001.

[13] L. Dormieux, A. Molinari, and D. Kondo, "Micromechanical approach to the behavior of poroelastic materials," *Journal of the Mechanics and Physics of Solids*, vol. 50, no. 10, pp. 2203–2231, 2002.

[14] T. Mori and K. Tanaka, "Average stress in matrix and average elastic energy of materials with misfitting inclusions," *Acta Metallurgica*, vol. 21, no. 5, pp. 571–574, 1973.

[15] Y. Benveniste, "A new approach to the application of Mori-Tanaka's theory in composite materials," *Mechanics of Materials*, vol. 6, no. 2, pp. 147–157, 1987.

[16] A. I. Lurje, *Räumliche Probleme der Elastizitätstheorie [Spatial problems of elasticity theory]*. Akademie Verlag Berlin, 1963, in German.

[17] D. Taylor, J. G. Hazenberg, and T. C. Lee, "The cellular transducer in damage-stimulated bone remodelling: a theoretical investigation using fracture mechanics," *Journal of Theoretical Biology*, vol. 225, no. 1, pp. 65–75, 2003.

[18] A. Fritsch, C. Hellmich, and L. Dormieux, "Ductile sliding between mineral crystals followed by rupture of collagen crosslinks: Experimentally supported micromechanical explanation of bone strength," *Journal of Theoretical Biology*, vol. 260, no. 2, pp. 230–252, 2009.
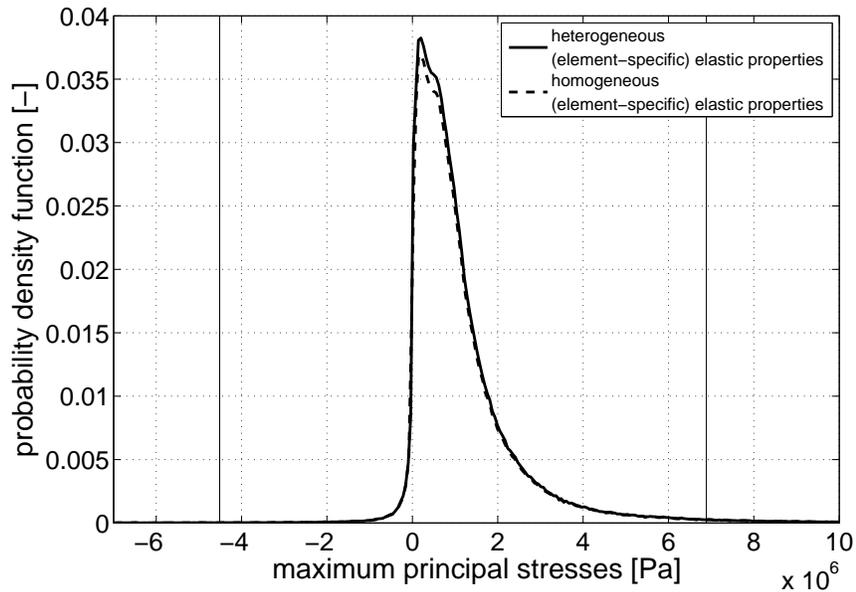
Figure 3: Solid Finite Elements-related probability density function of maximum principal stresses: comparison of heterogeneous (solid line) and homogeneous (dashed line) simulation. 99% of all principal stress values lie between the two vertical lines
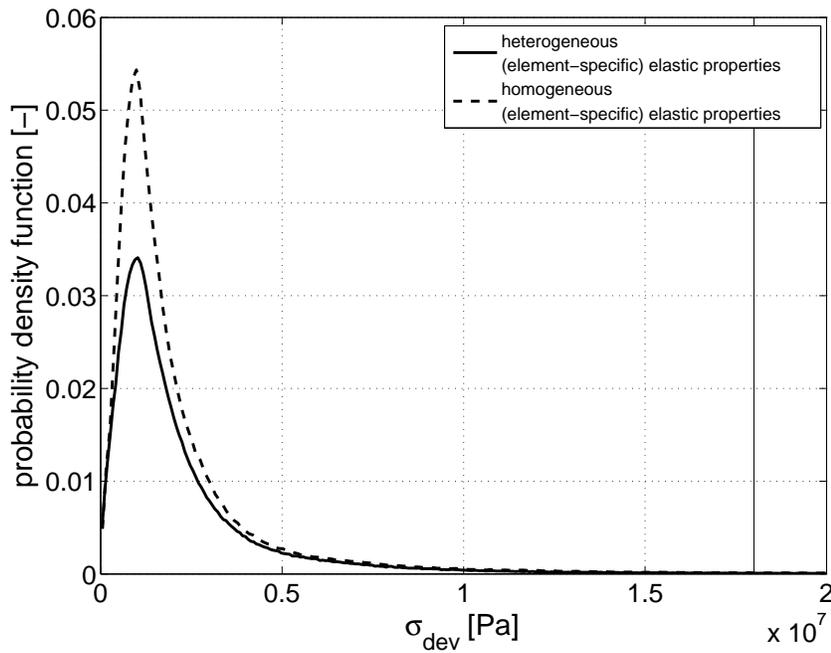

Figure 4: Solid Finite Elements-related probability density function of deviatoric stress norms: comparison of heterogeneous (solid line) and homogeneous (dashed line) simulations. 99% of all deviatoric stress norm values lie below the vertical line
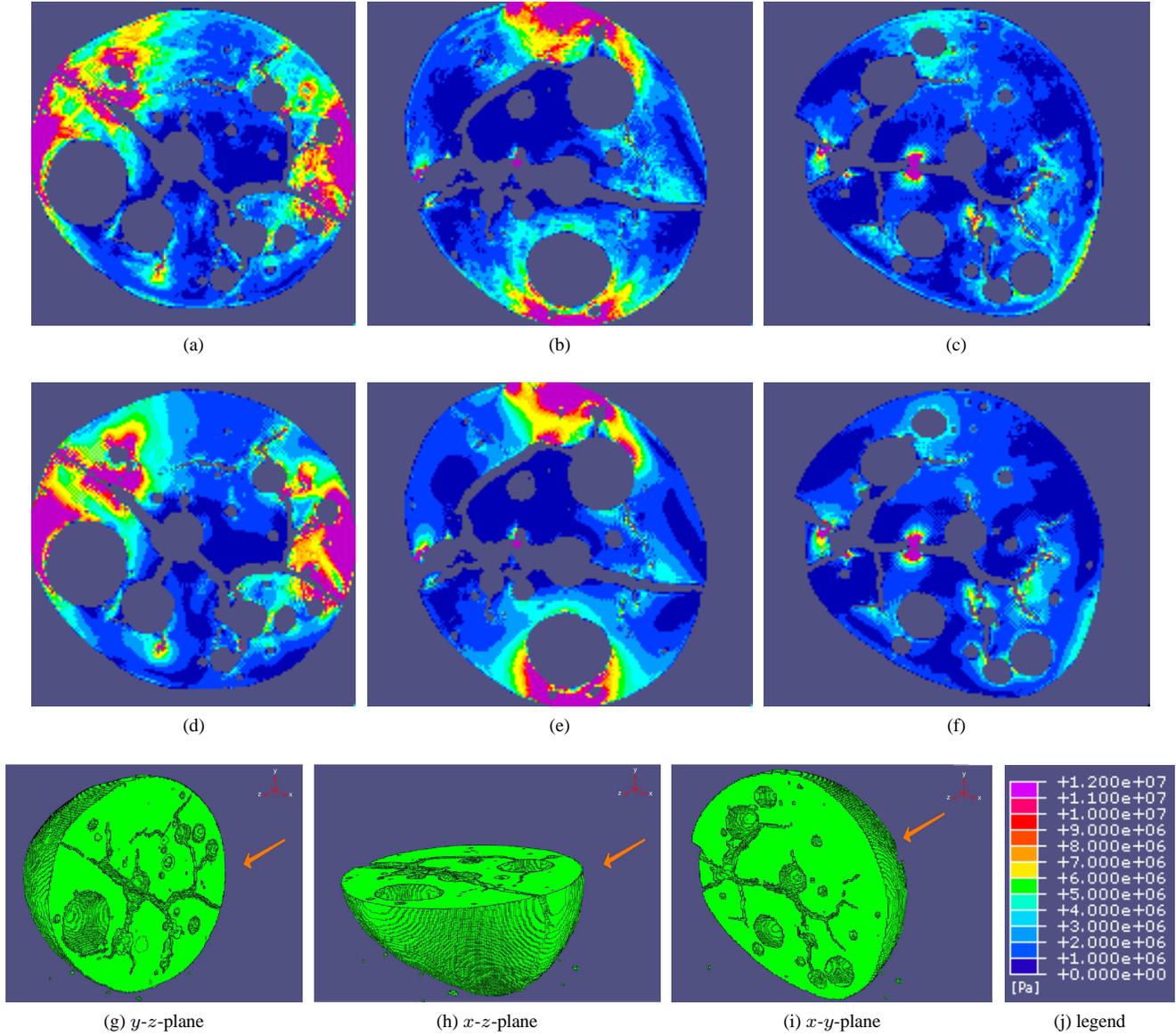
Figure 5: Results of FE simulation, with (element-specific) heterogeneous [(a), (b), (c)] and homogeneous [(d), (e), (f)] elastic properties: deviatoric stress norms σ_{dev} [Pa], in three perpendicular cross sections through the center of the granule. The cross sections are parallel to the y-z (g), x-z (h), and, x-y (i) planes. 97.92% of all values lie between 0 and 12 MPa [see color legend (j)]
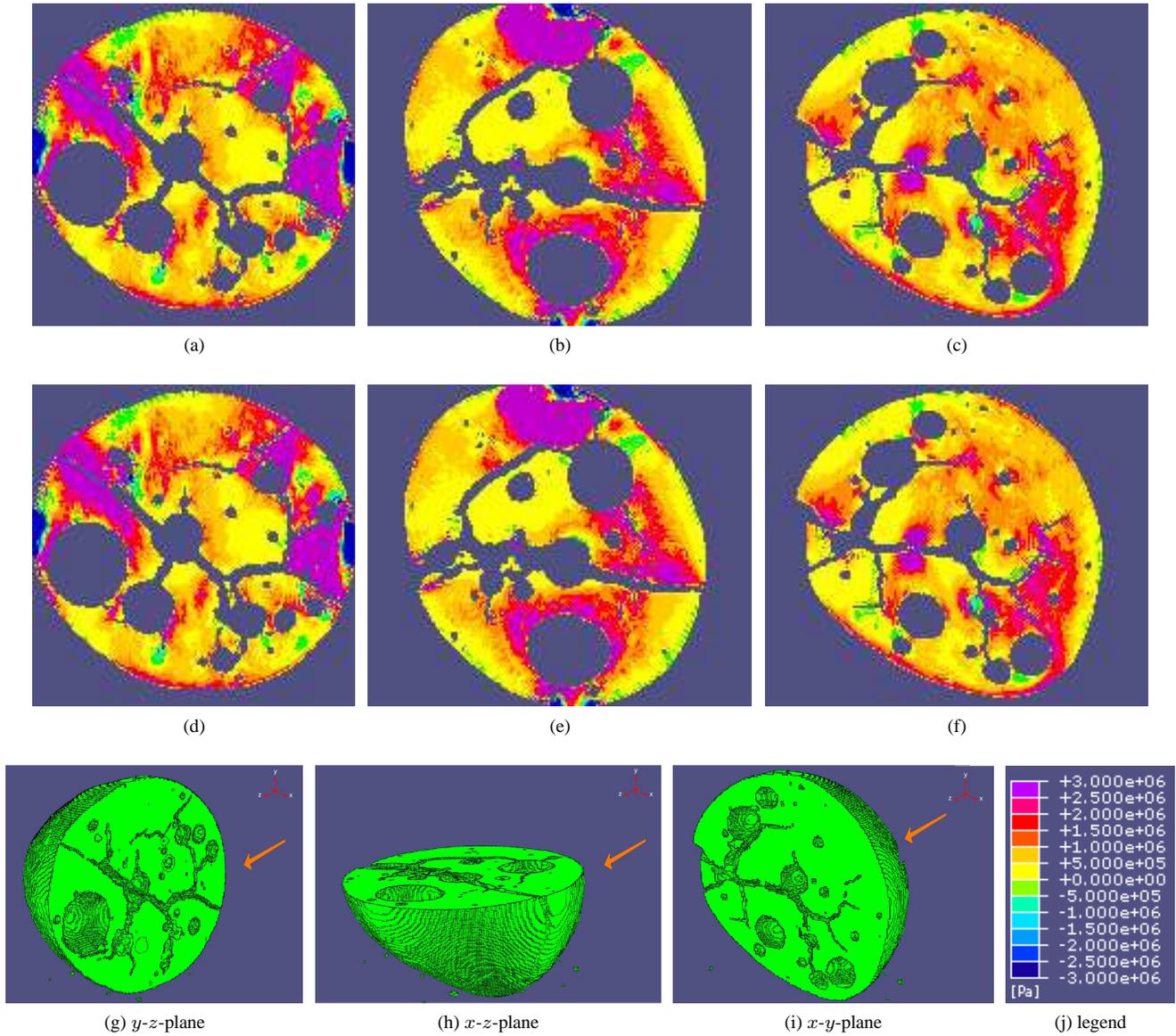
Figure 6: Results of FE simulation, with (element-specific) heterogeneous [(a), (b), (c)] and homogeneous [(d), (e), (f)] elastic properties: maximum principal stresses (maximum eigenvalue of $\boldsymbol{\sigma}$) [Pa], in three perpendicular cross sections through the center of the granule. The cross sections are parallel to the y-z (g), x-z (h), and, x-y (i) planes. 95.90% of all values lie between $\pm$ 3 MPa [see color legend (j)]